Localized-delocalized transition of the exciton and scaling description of phase-conjugated wave generation

Nobuhiko Taniguchi and Eiichi Hanamura
Department of Applied Physics, University of Tokyo, Hongo, Bunkyo-ku, Tokyo 113, Japan
(Received 17 November 1992)

Under nearly resonant pumping of Frenkel excitons, the third-order optical process generating phase-conjugated waves is theoretically investigated by taking full account of the effect due to static on-site disorder and finite sample size. The scaling theory of the Anderson localization allows us to show that the phase-conjugated signal has the spectral anomaly for pump and probe frequencies around the exciton mobility edge. We systematically evaluate the dependence of the phase-conjugated signal on various physical quantities, namely, randomness, the detuning of the pump and probe frequencies from the exciton mobility edge, the misalignment of two pump beams, and the system size.

I. INTRODUCTION

Currently there is increasing interest in the nonlinear optical properties of the organic and inorganic crystals. In particular, much attention is focused on various nonlinear optical responses of the exciton in these systems. An ideal exciton is an elementary electronic excitation that extends and can propagate coherently over the whole crystal. Both the finite sample size and the relaxation of the exciton limit its coherent length to a mesoscopic size, and consequently the effective transition dipole moment of the exciton, are also reduced to a mesoscopic value. In a system of semiconductor microcrystallites, the finite-size effect is known as the confinement effect of an exciton, which leads to the third-order susceptibility being proportional to the volume of the semiconductor microcrystallite under resonant pumping of excitons.[1,2] In the disordered system with random on-site energies, the exciton scattering gives the pure dephasing processes and reduces the effective dipole moment of an exciton.[3,4] On the other hand, the importance of coherent multiple scattering by static random potentials has recently been recognized in nonlinear optical properties, and a weak localization effect in disordered systems has been shown to enhance the generation of the phase-conjugated waves in nearly degenerate four-wave mixing.[5–9] It should be emphasized that disorder in the system gives both the positive and negative effects for getting large nonlinear optical responses. Complicating the situation, furthermore, finiteness of the sample destroys the weak localization effect. In order to take full account of these disorder effects in Frenkel exciton systems properly, we use a well-defined microscopic model for disorder and its scaling theory of localization in order to examine the disordered and finite-size effects on the same basis. We clarify the nature of phase-conjugated wave generation in the disordered and finite system.

Another interesting problem is about the localized-delocalized transition of the exciton in the frequency domain. Such a transition point is called the mobility edge, where the states of the exciton change in nature from the localized to the extended states or vice versa. It is noted that the exciton wave number is not a good quantum number in this system, so that the linear absorption spectrum due to the exciton is very broad and almost constant around the mobility edge. Nonlinear optical responses such as (stimulated) Raman-scattering processes have been observed around the exciton mobility edge ω^* under nearly resonant pumping of excitons.[10,11] Nontrivial nature is expected around the exciton mobility edge because the exciton's correlation (localization) length diverges when pump and probe frequencies approach the mobility edge in the delocalized (localized) phase. Divergence of the localization length implies that the effective transition dipole moment of an exciton will become very large at that point irrespective of a rather large pure dephasing rate by impurity scatterings. The confinement effect of excitons and the misalignment of forward and backward beams also play a crucial role here, because both finiteness of the system and the misalignment are known to smear out the critical behavior around the transition point. To investigate such singular behavior in nonlinear polarization around the exciton mobility edge, incorporating all these various effects fairly upon the same basis, we resort to the scaling theory of localization.[12,13] A commonly used method is the perturbational calculation of exciton scattering by a random potential breakdown, particularly around the exciton mobility edge. We develop the length-dependent scaling theory for the enhancement factor of phase-conjugated wave generation and examine its behavior on both the localized and the delocalized sides of the exciton mobility edge. As a result, we obtain the following: (1) spectral singularity will occur at the exciton mobility edge, and (2) a different singular behavior of the enhancement factor for the phase-conjugated signal is expected on both sides of the exciton mobility edge. Putting it the other way round, localization and delocalization of the exciton, which is

still an open problem, can be studied by observing the generation of phase-conjugated waves, when the pump- and probe-beam frequencies are close to the exciton mobility edge and still under nearly resonant pumping of excitons.

In investigating the exciton propagation in the disordered medium, two diffusion modes are relevant: the particle-hole mode (diffuson) and the particle-particle mode (cooperon).[13] Whereas the diffuson mode corresponds to the forward coherent-scattering process, the cooperon mode describes that the backward-scattering amplitude is enhanced by multiple impurity scatterings as a result of constructive interference between two processes that are connected with each other by time-reversal symmetry. Since the phase conjugation is a process generating a wave whose phase is a complex conjugate to the incident probe wave, it is very natural that nonlinear polarization for the phase conjugation is expressed by use of the cooperon mode.[5–9] In later sections, when the incident waves are under resonant pumping of the exciton, we will find that the enhancement factor $N_{\rm eff}$ for the phase-conjugated signal is directly written down by the cooperon mode with the momentum and the frequency specified by the external electric field.

According to the scaling argument of Anderson localization in conductors, all the states are localized in a one- and two-dimensional bulk system at the absolute-zero temperature, and the localized-delocalized transition is expected to occur in the three-dimensional system. Such a localization effect of an exciton can be described through the interaction between the two diffusion modes.[13,14] The diffusion modes can be formulated as Goldstone modes, and several kinds of nonlinear σ models are introduced to pursue the localization problem along this line.[14–18] As is shown in the framework of the nonlinear σ model, the disorder effect of diffusion modes in the delocalized side of the exciton mobility edge is incorporated through the renormalized diffusion coefficient. This nontrivial feature of the Anderson localization theory is based upon the nonvanishing of the averaged density of states, that is, an order parameter, at the transition point. As the exciton's average density of states is not expected to vanish at the exciton mobility edge, we rely fairly upon this insight. Thus we apply the length-dependent scaling law to the diffuson (cooperon) mode. This allows us to investigate the disorder effect and the finite-size effect on the enhancement factor $N_{\rm eff}$ for phase-conjugated wave generation in terms of the correlation (localization) length.

We start from the microscopic Hamiltonian of Frenkel excitons with static on-site disorder in Sec. II. The longitudinal damping of an exciton into the ground state is included phenomenologically in the form of the Liouville operator. In Sec. III we formulate a linear optical response and nonlinear polarizations for phase-conjugated wave generation. The dominant contribution for the third-order susceptibility is examined under nearly resonant pumping of excitons in Sec. IV. We perform the perturbational expansion from the delocalized limit. The relation between the enhancement factor for the phase conjugation and the cooperon mode is explicitly shown. In Sec. V we develop the length-dependent scaling theory for the enhancement factor of the phase-conjugated wave generation. The spectral anomaly of this signal around the exciton mobility edge is demonstrated. Its dependence on the system size and the misalignment is also examined. In Sec. VI we summarize our results, and discuss how to observe the localized-delocalized transition in frequency by observing the phase-conjugated wave generation as a function of pump frequency or of the misalignment of two pump beams.

II. MICROSCOPIC MODEL

We start from the microscopic model for Frenkel excitons in N-coupled two-level atoms (or molecules) with random on-site energies Ω_i and dipolar couplings between them (see also Refs. 8 and 9). The volume of the system is defined as $V = L^d$ (L is a system size in dimension d). The time evolution of the density matrix $\varrho(t)$ of the electronic system is determined by the following Liouville equation ($\hbar = 1$ here and hereafter):

$$\frac{d\varrho}{dt} = -i[H_0 + H'(t), \varrho] + \mathcal{L}_\gamma \varrho, \tag{1}$$

where H_0 is the Hamiltonian of the electronic system and $H'(t)$ is the interaction between the electronic system and the transverse electric fields $\mathbf{E}^\perp(\mathbf{r},t)$. In terms of Pauli spin operators S_i^+ (S_i^-) creating (annihilating) the excitation at the site i, the Hamiltonians H_0 and $H'(t)$ are expressed by

$$H_0 = \sum_{(i,j)} T(\mathbf{r}_i - \mathbf{r}_j)\, S_i^+ S_j^-, \tag{2a}$$

$$H'(t) = -\int d\mathbf{r}\, \hat{\mathbf{P}}(\mathbf{r}) \cdot \mathbf{E}^\perp(\mathbf{r},t). \tag{2b}$$

The electronic dipole-moment density operator $\hat{\mathbf{P}}(\mathbf{r})$ is given by

$$\hat{\mathbf{P}}(\mathbf{r}) = \sum_i \boldsymbol{\mu}(S_i^+ + S_i^-)\delta(\mathbf{r} - \mathbf{r}_i), \tag{3}$$

with $\boldsymbol{\mu}$ the atomic transition dipole moment. The term $T(\mathbf{r}_i - \mathbf{r}_j)$ in the Hamiltonian H_0 describes the random on-site energy Ω_i for $i = j$ and the dipolar couplings for $i \neq j$. The on-site energies Ω_i are assumed to obey the Gaussian probability distribution with the average

$$\langle \Omega_i \rangle_{\rm av} = \Omega_0, \tag{4a}$$

and the variance

$$\langle \Omega_i\, \Omega_j \rangle_{\rm av} - \langle \Omega_i \rangle_{\rm av} \langle \Omega_j \rangle_{\rm av} = W^2 \delta_{i,j}. \tag{4b}$$

For convenience, we introduce the ground state $|g\rangle$, one-exciton eigenstates $|\alpha\rangle$, and two-exciton eigenstates $|(\sigma\sigma')\rangle$ of Hamiltonian H_0. Because of Pauli's exclusion principle, there are N one-exciton eigenstates and $N(N-1)/2$ two-exciton eigenstates. We designate the eigenenergies of these states as

$$H_0 |g\rangle = 0, \tag{5a}$$

$$H_0 |\alpha\rangle = \Omega_\alpha |\alpha\rangle, \tag{5b}$$

$$H_0 |(\sigma\sigma')\rangle = \Omega_{\sigma\sigma'} |(\sigma\sigma')\rangle. \tag{5c}$$

The Liouville operator $\mathcal{L}_\gamma \varrho$ in Eq. (1) describes the relaxation processes of excited states into the ground state. As is shown later, it suffices to consider only matrix elements involving one-exciton eigenstates and the ground state under resonant pumping of excitons (see also Ref. 8). However, for completeness, we here assume a rather general form for the Liouville operator $\mathcal{L}_\gamma \varrho$ as:

$$\langle g|\,\mathcal{L}_\gamma \varrho\,|g\rangle \cong 2\sum_\alpha \gamma_\alpha \varrho_{\alpha,\alpha} + 2\sum_{(\sigma\sigma')} \gamma_{\sigma\sigma'} \varrho_{\sigma\sigma',\sigma\sigma'}, \tag{6a}$$

$$\langle \alpha|\,\mathcal{L}_\gamma \varrho\,|g\rangle \cong -\gamma_\alpha \varrho_{\alpha,g}, \tag{6b}$$

$$\langle \alpha|\,\mathcal{L}_\gamma \varrho\,|\beta\rangle \cong -(\gamma_\alpha+\gamma_\beta)\varrho_{\alpha,\beta}, \tag{6c}$$

$$\langle (\sigma\sigma')|\,\mathcal{L}_\gamma \varrho\,|g\rangle \cong -\gamma_{\sigma\sigma'}\,\varrho_{\sigma\sigma',g}, \tag{6d}$$

$$\langle (\sigma\sigma')|\,\mathcal{L}_\gamma \varrho\,|\alpha\rangle \cong -(\gamma_{\sigma\sigma'}+\gamma_\alpha)\varrho_{\sigma\sigma',\alpha}, \tag{6e}$$

$$\langle (\sigma_1\sigma_1')|\,\mathcal{L}_\gamma \varrho\,|(\sigma_2\sigma_2')\rangle \cong -(\gamma_{\sigma_1\sigma_1'}+\gamma_{\sigma_2\sigma_2'})\varrho_{\sigma_1\sigma_1',\sigma_2\sigma_2'}. \tag{6f}$$

It can be easily confirmed that the relaxation matrix $\mathcal{L}_\gamma \varrho$ introduced above conserves the probability. The solution $\varrho(t)$ of the Liouville Eq. (1) always satisfies the identity

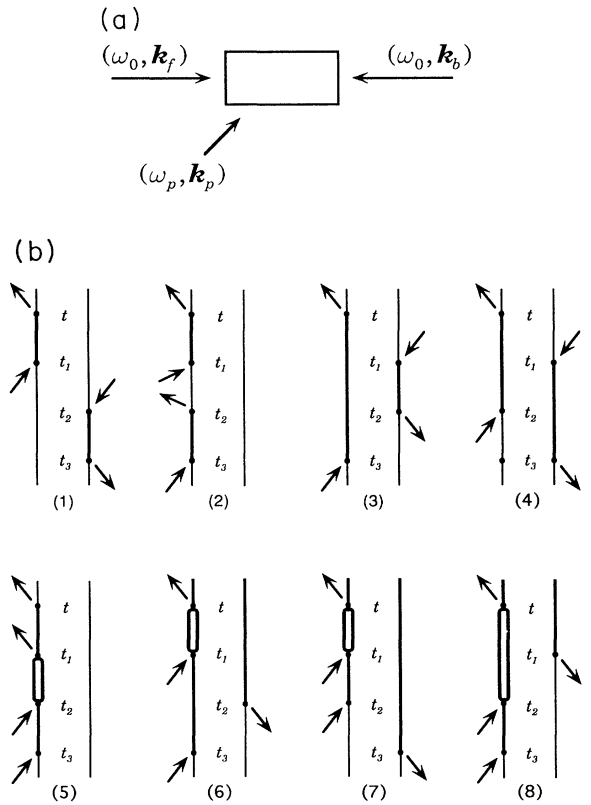

FIG. 1. (a) The geometry of the nearly degenerate four-wave mixing. Three incident beams are used: the forward (backward) pump beams denoted by $(\omega_0, \mathbf{k}_{f(b)})$, and the probe beam by $(\omega_p, \mathbf{k}_p)$. The signal beam phase conjugated to the probe light is observed at $(\omega_s, \mathbf{k}_s) = (2\omega_0 - \omega_p, \mathbf{k}_f + \mathbf{k}_b - \mathbf{k}_p)$. (b) All the processes contributing to the third-order nonlinear polarization under the rotating-wave approximation in the double Feynman diagrams. The thick line and the double line denote the one-exciton and two-exciton states, respectively.

$\mathrm{Tr}\varrho(t) = 1$, so that we come across no unphysical divergences in the nonlinear susceptibility arising from the lack of conservation of probability.[19] In later sections we assume that the relaxation rates γ_α are independent of the state, and much smaller than the pure dephasing rate γ' due to impurity, i.e., $\gamma_\alpha = \gamma \ll \gamma'$. It is noted that the effect of the pure dephasing processes is taken account of, not in the relaxation matrix $\mathcal{L}_\gamma \varrho$, but in the Hamiltonian H_0. The pure dephasing rate γ' is evaluated by the Born approximation of impurity scattering in Sec. IV. Corresponding to the experimental setting shown in Fig. 1(a), the external electric field inducing the phase-conjugated signal by a nearly degenerate four-wave mixing is decomposed into the three incident beams,

$$\mathbf{E}^{\perp}(\mathbf{r},t) = \sum_{l=1}^{3} \left(\mathbf{E}_l e^{i\mathbf{k}_l\cdot\mathbf{r}-i\omega_l t} + \mathbf{E}_l^* e^{-i\mathbf{k}_l\cdot\mathbf{r}+i\omega_l t}\right). \tag{7}$$

Here $(\omega_l, \mathbf{k}_l)$ $(l = 1,2,3)$ denote the forward $(\omega_0, \mathbf{k}_f)$ and backward $(\omega_0, \mathbf{k}_b)$ pump beams, and the probe beam $(\omega_p, \mathbf{k}_p)$. We observe the signal beam phase conjugated to the incident probe light at $(\omega_s, \mathbf{k}_s) = (2\omega_0 - \omega_p, \mathbf{k}_f + \mathbf{k}_b - \mathbf{k}_p)$.

III. LINEAR AND NONLINEAR SUSCEPTIBILITIES

In this section we briefly survey how linear and nonlinear optical polarizations and susceptibilities are evaluated. Though our interest is focused much upon the nearly degenerate four-wave mixing under resonant exciton pumping, the results in this section are general. The electronic polarization of the system is calculated through the solution $\varrho(t)$ of Eq. (1) as

$$\mathbf{P}(\mathbf{r},t) = \langle \mathrm{Tr}\{\hat{\mathbf{P}}(\mathbf{r})\,\varrho(t)\}\rangle_{\mathrm{av}}. \tag{8}$$

It is important that we take the ensemble average $\langle\,\rangle_{\mathrm{av}}$ of the physical quantity over the random configuration of on-site energies. We evaluate linear and nonlinear polarizations by expanding the density matrix $\varrho(t)$ in $H'(t)$ to the third-order in a rotating-wave approximation. The Liouville equation can be formally rewritten as

$$\frac{\partial}{\partial t}\varrho = \mathcal{L}_0\,\varrho + \mathcal{L}_1(t)\,\varrho, \tag{9}$$

where we introduce the Liouville operators $\mathcal{L}_0$ and $\mathcal{L}_1(t)$ by

$$\mathcal{L}_0 = -i\,[H_0,\,\cdot\,] + \mathcal{L}_\gamma, \tag{10a}$$

$$\mathcal{L}_1(t) = -i\,[H'(t),\,\cdot\,]. \tag{10b}$$

The formal solution of Eq. (9) is given by

$$\varrho(t) = \mathcal{U}(t,-\infty)\,\varrho(-\infty), \tag{11}$$

where the operator $\mathcal{U}$ in the Liouville space is expressed with the time-ordered exponential as

$$\mathcal{U}(t,t') = e^{\mathcal{L}_0 t}\,T\exp\left[\int_{t'}^{t}\tilde{\mathcal{L}}_1(t_1)dt_1\right]\,e^{-\mathcal{L}_0 t'}, \tag{12}$$

with $\tilde{\mathcal{L}}_1(t) \equiv e^{-\mathcal{L}_0 t}\,\mathcal{L}_1(t)\,e^{\mathcal{L}_0 t}$. At time $t \to -\infty$, we as-

sume the electronic system to be at the ground state: $\varrho(-\infty) = \varrho_0 \equiv |g\rangle\langle g|$. The interaction $H'(t)$ is adiabatically switched on. By expanding the time-ordered exponential, we obtain the density matrix expanded in a perturbation series of $H'(t)$,

$$\varrho(t) = \varrho^{(0)}(t) + \varrho^{(1)}(t) + \varrho^{(2)}(t) + \varrho^{(3)}(t) + \cdots, \tag{13}$$

where

$$\varrho^{(0)}(t) = \varrho_0, \tag{14a}$$

$$\varrho^{(1)}(t) = e^{\mathcal{L}_0 t}\int_{-\infty}^{t} dt_1 \tilde{\mathcal{L}}_1(t_1)\,\varrho_0, \tag{14b}$$

$$\varrho^{(2)}(t) = e^{\mathcal{L}_0 t}\int_{-\infty}^{t} dt_1 \int_{-\infty}^{t_1} dt_2 \tilde{\mathcal{L}}_1(t_1)\tilde{\mathcal{L}}_1(t_2)\,\varrho_0, \tag{14c}$$

$$\varrho^{(3)}(t) = e^{\mathcal{L}_0 t}\int_{-\infty}^{t} dt_1 \int_{-\infty}^{t_1} dt_2 \int_{-\infty}^{t_2} dt_3 \tilde{\mathcal{L}}_1(t_1)\tilde{\mathcal{L}}_1(t_2) \times \tilde{\mathcal{L}}_1(t_3)\,\varrho_0. \tag{14d}$$

Linear and nonlinear polarizations (and susceptibilities) are defined using the density matrices $\varrho^{(1)}(t)$ and $\varrho^{(3)}(t)$ as

$$\mathbf{P}^{(1)}(\mathbf{r},t) = \mathrm{Tr}\{\hat{\mathbf{P}}(\mathbf{r})\,\varrho^{(1)}(t)\}, \tag{15a}$$

$$\mathbf{P}^{(3)}(\mathbf{r},t) = \mathrm{Tr}\{\hat{\mathbf{P}}(\mathbf{r})\,\varrho^{(3)}(t)\}, \tag{15b}$$

and the second-order nonlinear polarization $\mathbf{P}^{(2)}(\mathbf{r},t)$ vanishes. Linear polarization is straightforwardly obtained under a rotating-wave approximation through Eq. (14b). It leads to

$$\mathbf{P}^{(1)}(\mathbf{r},t) = -\frac{N}{V}\sum_{\mathbf{k}_s}\sum_{l=1}^{3}\chi^{(1)} : \mathbf{E}_l e^{i\mathbf{k}_s\cdot\mathbf{r}-i\omega_l t} + \text{c.c.}, \tag{16}$$

where $\chi^{(1)}$ is a linear susceptibility and is given by

$$\chi^{(1)} = \left\langle \sum_{\alpha} \frac{\boldsymbol{\mu}\boldsymbol{\mu}\,\langle \mathbf{k}_s \mid \alpha\rangle\langle\alpha \mid \mathbf{k}_l\rangle}{\omega_l - \Omega_\alpha + i\gamma_\alpha} \right\rangle_{\mathrm{av}}. \tag{17}$$

Similarly nonlinear polarization can be obtained through Eqs. (14d) and (15b). Using $(\omega_s, \mathbf{k}_s) = (\omega_l - \omega_m + \omega_n, \mathbf{k}_l - \mathbf{k}_m + \mathbf{k}_n)$, we obtain after a small amount of calculation

$$\mathbf{P}^{(3)}(\mathbf{r},t) = \sum_{\mathbf{k}_s}\sum_{l,m,n=1}^{3}\chi^{(3)} : \mathbf{E}_l\mathbf{E}_m^*\mathbf{E}_n e^{i\mathbf{k}_s\cdot\mathbf{r}-i\omega_s t} + \text{c.c.}, \tag{18}$$

with

$$\chi^{(3)} = \chi^{(3)}_{1+2} + \chi^{(3)}_{3+4} + \chi^{(3)}_{5} + \chi^{(3)}_{6+7} + \chi^{(3)}_{8}. \tag{19}$$

The third-order susceptibility $\chi^{(3)}$ consists of five terms from eight diagrams depicted in Fig. 1(b): each suffix of $\chi^{(3)}_i$ denotes the contribution from ith diagram of Fig. 1(b). (See also, e.g., Ref. 20.) A detailed form of each term is given as follows:

$$\chi^{(3)}_{1+2} = \frac{N^2}{V}\left\langle \sum_{\alpha,\beta} \frac{\boldsymbol{\mu}\boldsymbol{\mu}\boldsymbol{\mu}\boldsymbol{\mu}\,\langle \mathbf{k}_s \mid \alpha\rangle\langle\alpha \mid \mathbf{k}_n\rangle\langle \mathbf{k}_m \mid \beta\rangle\langle\beta \mid \mathbf{k}_l\rangle}{(\omega_s - \Omega_\alpha + i\gamma_\alpha)(\omega_l - \Omega_\beta + i\gamma_\beta)(\omega_m - \Omega_\beta - i\gamma_\beta)} \right\rangle_{\mathrm{av}}, \tag{20a}$$

$$\chi^{(3)}_{3+4} = \frac{N^2}{V}\left\langle \sum_{\alpha,\beta} \frac{\boldsymbol{\mu}\boldsymbol{\mu}\boldsymbol{\mu}\boldsymbol{\mu}\,\langle \mathbf{k}_s \mid \alpha\rangle\langle\alpha \mid \mathbf{k}_n\rangle\langle \mathbf{k}_m \mid \beta\rangle\langle\beta \mid \mathbf{k}_l\rangle}{(\omega_s - \Omega_\alpha + i\gamma_\alpha)(\omega_n - \Omega_\alpha + i\gamma_\alpha)(\omega_m - \Omega_\beta - i\gamma_\beta)} \right\rangle_{\mathrm{av}}, \tag{20b}$$

$$\chi^{(3)}_{5} = -\frac{N^2}{V}\left\langle \sum_{\alpha,\beta,(\sigma\sigma')} \frac{\boldsymbol{\mu}\boldsymbol{\mu}\boldsymbol{\mu}\boldsymbol{\mu}\,\langle \mathbf{k}_s \mid \alpha\rangle\langle\alpha\mathbf{k}_m \mid (\sigma\sigma')\rangle\langle(\sigma\sigma') \mid \beta\mathbf{k}_n\rangle\langle\beta \mid \mathbf{k}_l\rangle}{(\omega_s - \Omega_\alpha + i\gamma_\alpha)(\omega_l + \omega_n - \Omega_{\sigma\sigma'} + i\gamma_{\sigma\sigma'})(\omega_l - \Omega_\beta + i\gamma_\beta)} \right\rangle_{\mathrm{av}}, \tag{20c}$$

$$\chi^{(3)}_{6+7} = -\frac{N^2}{V}\left\langle \sum_{\alpha,\beta,(\sigma\sigma')} \frac{\boldsymbol{\mu}\boldsymbol{\mu}\boldsymbol{\mu}\boldsymbol{\mu}\,\langle \mathbf{k}_m \mid \alpha\rangle\langle\alpha\mathbf{k}_s \mid (\sigma\sigma')\rangle\langle(\sigma\sigma') \mid \beta\mathbf{k}_n\rangle\langle\beta \mid \mathbf{k}_l\rangle}{(\omega_s + \Omega_\alpha - \Omega_{\sigma\sigma'} + i\gamma_\alpha + i\gamma_{\sigma\sigma'})(\omega_l - \Omega_\alpha + i\gamma_\alpha)(\omega_m - \Omega_\beta - i\gamma_\beta)} \right\rangle_{\mathrm{av}}, \tag{20d}$$

$$\chi^{(3)}_{8} = \frac{N^2}{V}\sum_{\alpha,\beta,(\sigma\sigma')}\left\langle \frac{\boldsymbol{\mu}\boldsymbol{\mu}\boldsymbol{\mu}\boldsymbol{\mu}\,\langle \mathbf{k}_m \mid \alpha\rangle\langle\alpha\mathbf{k}_s \mid (\sigma\sigma')\rangle\langle(\sigma\sigma') \mid \beta\mathbf{k}_n\rangle\langle\beta \mid \mathbf{k}_l\rangle}{(\omega_s + \Omega_\alpha - \Omega_{\sigma\sigma'} + i\gamma_\alpha + i\gamma_{\sigma\sigma'})(\omega_l + \omega_n - \Omega_{\sigma\sigma'} + i\gamma_{\sigma\sigma'})(\omega_l - \Omega_\beta + i\gamma_\beta)} \right\rangle_{\mathrm{av}}. \tag{20e}$$

Here we use the notation of $|\mathbf{k}\rangle \equiv \sum_i \langle i \mid \mathbf{k}\rangle\, S_i^+ \,|g\rangle$ and $|\beta\mathbf{k}\rangle \equiv S_\beta^+ \,|\mathbf{k}\rangle = \sum_\beta \langle i \mid \beta\rangle\, S_i^+ \,|\mathbf{k}\rangle$. The third-order optical susceptibility should be proportional to atomic density N/V for the bulk material. It should be emphasized that the expressions obtained above include all the effects due to disorder and finite sample size. What is difficult lies in obtaining the eigenstates of the Hamiltonian H_0 and making the ensemble average over random impurity configuration. In the following section, we show that such difficulty will be overcome under resonant pumping of excitons. We will find the factor N^2/V in the expression of $\chi^{(3)}$ to be reduced to $(N/V)\,N_{\mathrm{eff}}$, where N_{eff} is the enhancement factor of the nonlinear optical polarization that we will define.

IV. RANDOM AVERAGED PERTURBATION THEORY

We investigate the disorder effect on linear and nonlinear optical susceptibilities. As stated previously, we neglect the state dependence of the relaxation rate into the ground state, and set all γ_α's to a constant γ. For simplicity, we assume all the external radiation fields have the same polarization, and designate the parallel component of the atomic transition dipole moment $\boldsymbol{\mu}$ as μ. We introduce the retarded and advanced Green functions by

$$\hat{G}^{R,A}(z) = [z - H_0 \pm i\gamma]^{-1}. \tag{21}$$

It is noted that the Green functions Eq. (21) are not c numbers but operators.

A. Disorder effect on linear susceptibility

To begin with, we examine the disorder effect on linear susceptibility $\chi^{(1)}$. Linear susceptibility can be expressed in terms of the Green function as

$$\chi^{(1)} = \mu^2 \langle \langle \mathbf{k}_s | \hat{G}^R(\omega_l) | \mathbf{k}_l \rangle \rangle_{\mathrm{av}}. \tag{22}$$

Thus evaluating linear susceptibility is reduced to that of the averaged retarded one-particle Green functions $G^R_{\mathbf{k}_s}(\omega_l)$, which is defined by

$$\langle \langle \mathbf{k}_s | \hat{G}^{R,A}(z) | \mathbf{k}_l \rangle \rangle_{\mathrm{av}} = G^{R,A}_{\mathbf{k}_s}(z)\, \delta_{\mathbf{k}_s,\mathbf{k}_l}. \tag{23}$$

The self-energy of the exciton $\Sigma^{R,A}_{\mathbf{k}}(\omega)$ is evaluated in the Born approximation as in Fig. 2(a). The imaginary part of the self-energy part $\Sigma^{R,A}_{\mathbf{k}}(\omega)$ will define the pure dephasing rate γ'. Neglecting the real part of $\Sigma^{R,A}_{\mathbf{k}}(\omega)$, which is an energy shift, we obtain

$$\begin{aligned}\Sigma^{R,A}_{\mathbf{k}}(\omega) &= \frac{W^2}{N} \sum_i \langle i | \hat{G}^{R,A}(\omega) | i \rangle \\ &= \mp i \pi N_0 W^2 \left(\frac{V}{N}\right) \equiv \mp i\gamma',\end{aligned} \tag{24}$$

where N_0 is the average state density of the exciton per unit volume at frequency ω_0. Thus the averaged retarded and advanced Green function is expressed by

$$G^{R,A}_{\mathbf{k}}(\omega) = [\omega - \Omega_{\mathbf{k}} \pm i(\gamma + \gamma')]^{-1}. \tag{25}$$

The symbol $\Omega_{\mathbf{k}}$ denotes the exciton's dispersion relation in the system without disorder. Hence linear susceptibility is evaluated as

$$\chi^{(1)} = \frac{\mu^2}{\omega_l - \Omega_{\mathbf{k}_l} + i(\gamma' + \gamma)}. \tag{26}$$

We find that the disorder effect on linear susceptibility merely gives the pure-dephasing rate due to scattering by impurities, as is expected. Thus no singular behavior of linear susceptibility is anticipated around the exciton mobility edge. We will show that disorder in the system will give quite a different effect on nonlinear susceptibility describing phase conjugation.

B. Disorder effect on phase-conjugated wave generation

What we are interested in is the third-order nonlinear susceptibility for phase conjugation under resonant pumping of excitons. The phase-conjugated signal is observed at $(\omega_s, \mathbf{k}_s) = (2\omega_0 - \omega_p, \mathbf{k}_f + \mathbf{k}_b - \mathbf{k}_p)$, and this process corresponds to the cases $(l,m,n) = (f,p,b)$ and (b,p,f) in Eq. (18). The pure dephasing rate γ' given by Eq. (24) is assumed to be much larger than γ, so that we retain the leading terms in the expansion of Eq. (18) in γ/γ' ($\ll 1$) under nearly resonant pumping of excitons.[8] The contribution coming from diagrams (1)–(4) in Fig. 1(b) becomes larger than that from (5)–(8) by the order of magnitude γ'/γ ($\gg 1$). It is because the former contribution has the factor γ in the denominator at the phase-conjugated wave generation, whereas the latter does not. (See also Ref. 21.) Thus the dominant contribution to the third-order optical polarization producing phase-conjugated waves is found as

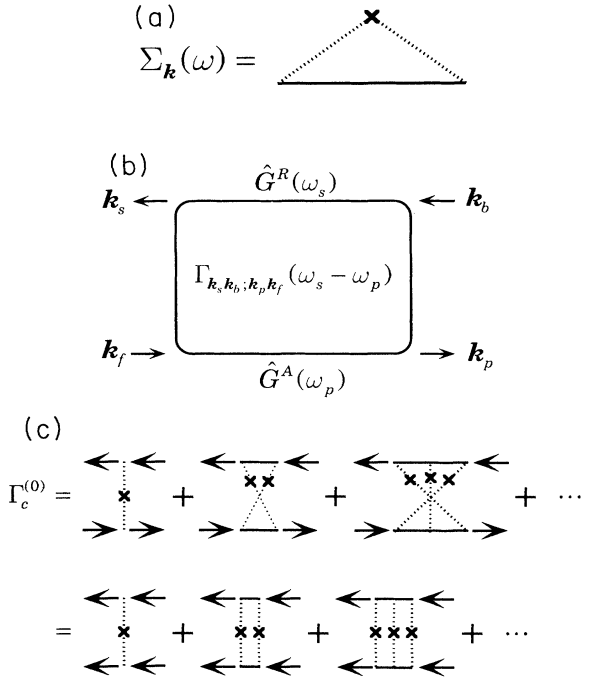

FIG. 2. (a) The self-energy of the averaged one-particle Green function. The dashed lines denote scattering of the exciton by the random on-site potential denoted by a cross. The random average is taken over the impurity position. (b) The general vertex part working between the retarded and the advanced Green functions. The vertex part depends also on the incident momenta $\mathbf{k}_f$, $\mathbf{k}_b$, and $\mathbf{k}_p$. (c) The lowest-order vertex part at $\mathbf{q} \equiv \mathbf{k}_f + \mathbf{k}_b \approx \mathbf{0}$—the lowest cooperon mode. If the direction of the advanced Green functions is reversed, the maximally crossed vertex part is transformed to the ladder vertex part. The figure shows that this vertex part is the bare diffusion propagator with the momentum singularity at $\mathbf{q} = \mathbf{0}$.

$$\chi^{(3)} \cong \chi^{(3)}_{1+2} + \chi^{(3)}_{3+4}. \tag{27}$$

We will show the dominant contribution to the third-order susceptibility given by Eq. (27) shows a singular behavior as a function of the detuning frequency $\delta\omega \equiv \omega_s - \omega_p$ and the misalignment between the forward and backward pump beams, $\mathbf{q} \equiv \mathbf{k}_f + \mathbf{k}_b$, when both are around zero. We introduce the enhancement factor $N_{\rm eff}$ for the generation of the phase-conjugated wave by

$$\chi^{(3)} = N_{\rm eff} \left(\frac{N}{V}\right) \frac{\mu^4}{(2i\gamma)} G^R_{\mathbf{k}_s}(\omega_s)\, G^A_{\mathbf{k}_p}(\omega_p). \tag{28}$$

The enhancement factor $N_{\rm eff}$ measures how many atoms (or molecules) can contribute coherently to the nonlinear optical polarization. To get the microscopic expression of the enhancement factor $N_{\rm eff}$, we rewrite Eqs. (20a) and (20b) in terms of the retarded and advanced Green functions introduced in Eq. (21) as follows:

$$\chi^{(3)}_{1+2} = \frac{N^2\mu^4}{V} \langle\langle \mathbf{k}_s|\hat{G}^R(\omega_s)|\mathbf{k}_n\rangle\langle\mathbf{k}_m|\hat{G}^R(\omega_l)\,\hat{G}^A(\omega_m)|\mathbf{k}_l\rangle\rangle_{\rm av}, \tag{29a}$$

$$\chi^{(3)}_{3+4} = \frac{N^2\mu^4}{V} \langle\langle \mathbf{k}_s|\hat{G}^R(\omega_s)\,\hat{G}^R(\omega_n)|\mathbf{k}_n\rangle\langle\mathbf{k}_m|\hat{G}^A(\omega_m)|\mathbf{k}_l\rangle\rangle_{\rm av}. \tag{29b}$$

Making use of the operator identities

$$\hat{G}^R(\omega_1)\hat{G}^A(\omega_2) = \frac{\hat{G}^A(\omega_2) - \hat{G}^R(\omega_1)}{\omega_1 - \omega_2 + 2i\gamma}, \tag{30a}$$

$$\hat{G}^R(\omega_1)\hat{G}^R(\omega_2) = \frac{\hat{G}^R(\omega_2) - \hat{G}^R(\omega_1)}{\omega_1 - \omega_2}, \tag{30b}$$

we can transform the terms $\chi^{(3)}_{1+2}$ and $\chi^{(3)}_{3+4}$ into the summation of the averaged two-body Green functions, and then decompose them into the form of the vertex part and the averaged one-body Green functions. As stated previously, we take only the terms whose behavior becomes singular in the generation of phase-conjugated waves at $\mathbf{k}_f + \mathbf{k}_b \approx \mathbf{0}$ and $\omega_s - \omega_p \approx 0$ in evaluating the optical nonlinear susceptibility $\chi^{(3)}$. Other terms that will be neglected here give the contribution of the order $(\xi_{\rm coh})^d N/V$ to $N_{\rm eff}$, where $\xi_{\rm coh} = [N_0(\gamma+\gamma')]^{-1/d}$ is the conventional coherent length of the exciton. This contribution is smaller by the order of magnitude γ/γ' ($\ll 1$) than that we retain. Consequently we obtain the microscopic expression of the enhancement factor $N_{\rm eff}$ for phase-conjugated wave generation as follows:

$$N_{\rm eff} = \left(\frac{N}{V}\right) \left[1 - 2i\gamma \frac{\partial}{\partial\,\delta\omega}\right] \Xi(\delta\omega)|_{\omega_s-\omega_p} + (f \leftrightarrow b), \tag{31}$$

$$\Xi(\omega_s - \omega_p) = G^R_{\mathbf{k}_b}(\omega_s)\, G^A_{\mathbf{k}_f}(\omega_p)\, \Gamma(\omega_s - \omega_p). \tag{32}$$

The vertex part $\Gamma(\omega_s - \omega_p)$, which is now constructed between the retarded and the advanced Green functions, depends also on the momenta of the three incident beams: $\mathbf{k}_f$, $\mathbf{k}_b$, and $\mathbf{k}_p$, as illustrated in Fig. 2(b). Hereafter we will call the function Ξ the coherent volume function. The vertex part $\Gamma(\omega_s - \omega_p)$ can be easily evaluated by the perturbational expansion from the delocalized limit as in Refs. 5 and 8. The diffusion mode called cooperon [Fig. 2(c); see also Ref. 13] is found to give the leading contribution at $\mathbf{q} = \mathbf{k}_f + \mathbf{k}_b \approx \mathbf{0}$, and $\delta\omega = \omega_s - \omega_p \approx 0$.[5,7,8] The cooperon mode depends only on $\delta\omega = \omega_s - \omega_p$ and $\mathbf{q} = \mathbf{k}_f + \mathbf{k}_b$ like

$$\Gamma^{(0)}_c(\delta\omega\,;\mathbf{q}) = \frac{\gamma'}{\pi N_0} \frac{2\gamma'}{D_0 q^2 - i\delta\omega + 2\gamma}, \tag{33}$$

where $D_0 \cong v_0^2/2d\gamma'$ is the bare diffusion coefficient and v_0 is the group velocity of the exciton. We obtain the lowest-order expression of the coherent volume function $\Xi(\delta\omega)$ under nearly resonant exciton pumping as a function of $\delta\omega$ and q:

$$\Xi^{(0)}(\delta\omega\,;\mathbf{q}) \cong \frac{2}{\pi} \frac{1}{N_0 D_0 q^2 + N_0(-i\delta\omega + 2\gamma)}. \tag{34}$$

The result shows that the coherent volume function for the completely phase-conjugated signal, i.e., $\delta\omega = 0$ and $\mathbf{q} = \mathbf{0}$ in Eq. (34), is dominated by 2γ and not by $\gamma + \gamma'$ in the delocalized limit.

V. SCALING DESCRIPTION OF PHASE-CONJUGATED WAVE GENERATION

A. Coherent volume function and renormalized cooperon

It is straightforward to evaluate the higher-order contribution for the vertex part $\Gamma(\omega_s - \omega_p)$.[13,15,16] It should be noted that the nonlinear σ model describes the physics of the diffusion mode, so that we calculate the higher correction corresponding to the one-loop calculation of the transverse correlation function in the nonlinear σ model. Here we follow the line of Ref. 13. The renormalized cooperon channel $\Gamma^{(1)}_c$ can be evaluated by use of the following Dyson equation as

$$\Gamma^{(1)}_c(\delta\omega\,;\mathbf{q}) = \Gamma^{(0)}_c(\delta\omega\,;\mathbf{q}) + \Gamma^{(0)}_c(\delta\omega\,;\mathbf{q})\,\Pi^{(1)}_c(\delta\omega\,;\mathbf{q})\,\Gamma^{(1)}_c(\delta\omega\,;\mathbf{q}). \tag{35}$$

The equation above can be schematically illustrated as shown in Fig. 3(a). We take the leading singular term for $\mathbf{q} \approx \mathbf{0}$ and $-i\delta\omega + 2\gamma \approx 0$. To perform the systematic expansion in W/T or $(4\pi^2 N_0 D_0 \ell^{d-2})^{-1}$, we find that $\Pi^{(1)}_c$ is expressed by the summation of the diagrams as in the Fig. 3(b). Each contribution can be written down explicitly as

$$\Pi^{(1)}_c = \Pi^{(1A)}_c + \Pi^{(1B)}_c + \Pi^{(1C)}_c, \tag{36}$$

where

$$\Pi_c^{(1A)}(\delta\omega;\mathbf{q}) = \sum_{\mathbf{Q}} \left[\left(\Gamma_d^{(0)}(\delta\omega;\mathbf{Q}) - \frac{\gamma'}{\pi N_0} \right) \sum_{\mathbf{k}} G^R_{\mathbf{k}+\mathbf{q}} G^R_{\mathbf{Q}-\mathbf{k}} G^A_{\mathbf{k}} G^A_{\mathbf{Q}-\mathbf{k}-\mathbf{q}} \right], \tag{37a}$$

$$\Pi_c^{(1B)}(\delta\omega;\mathbf{q}) = \frac{\gamma'}{\pi N_0} \sum_{\mathbf{Q}} \Gamma_d^{(0)}(\delta\omega;\mathbf{Q}) \left(\sum_{\mathbf{k}} G^R_{\mathbf{k}+\mathbf{q}} G^R_{\mathbf{Q}-\mathbf{k}} G^A_{\mathbf{k}} \right)^2, \tag{37b}$$

$$\Pi_c^{(1C)}(\delta\omega;\mathbf{q}) = \frac{\gamma'}{\pi N_0} \sum_{\mathbf{Q}} \Gamma_d^{(0)}(\delta\omega;\mathbf{Q}) \left(\sum_{\mathbf{k}} G^R_{\mathbf{k}} G^A_{\mathbf{Q}-\mathbf{k}} G^A_{\mathbf{k}-\mathbf{q}} \right)^2. \tag{37c}$$

The straightforward evaluation of the integrals leads to

$$\Pi_c^{(1)}(\delta\omega;\mathbf{q}) \cong \frac{\pi N_0}{4\gamma'^4} D_0 q^2 \sum_{\mathbf{Q}} \Gamma_d^{(0)}(\delta\omega;\mathbf{Q}). \tag{38}$$

Thus the renormalized cooperon mode $\Gamma_c^{(1)}(\delta\omega;\mathbf{q})$ is expressed by

$$\Gamma_c^{(1)}(\delta\omega;\mathbf{q}) = \frac{\gamma'}{\pi N_0} \frac{2\gamma'}{D_0(1-\Delta)q^2 - i\delta\omega + 2\gamma}, \tag{39}$$

$$\Delta = \frac{1}{\pi N_0} \int_{1/L}^{1/\ell} \frac{1}{D_0 Q^2 - i\delta\omega + 2\gamma} \frac{d^d Q}{(2\pi)^d}. \tag{40}$$

The correction Δ is found to be logarithmic in the two-dimensional bulk system as

$$\Delta = \frac{1}{4\pi^2 N_0 D_0} \ln \left[\frac{2\gamma'}{-i\delta\omega + 2\gamma} \right]. \tag{41}$$

This kind of logarithmic correction in the two-dimensional bulk system is characteristic in the localization theory.

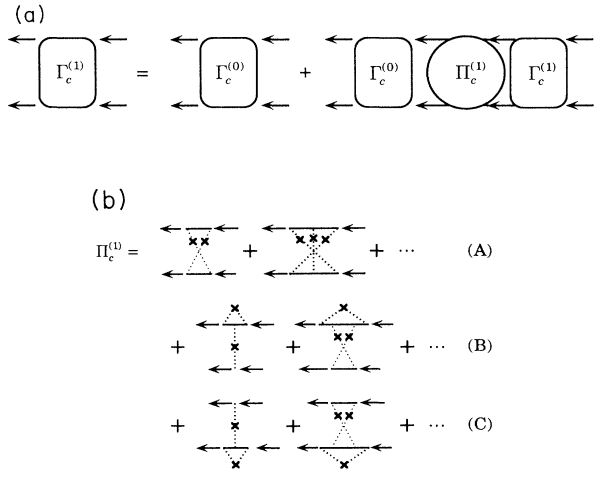

FIG. 3. Construction of the next higher order of the cooperon mode. (a) The Dyson equation is schematically illustrated, corresponding to Eq. (35). (b) Diagrammatic representation of $\Pi_c^{(1)} = \Pi_c^{(1A)} + \Pi_c^{(1B)} + \Pi_c^{(1C)}$ given by Eqs. (36)–(38). The summation of series of diagrams (A), (B), and (C) is written, respectively, by $\Pi_c^{(1A)}$, $\Pi_c^{(1B)}$, and $\Pi_c^{(1C)}$.

B. Scaling form of the coherent volume function

If the disorder in the system increases, the localization transition is caused by the interacting diffusion modes in the three-dimensional system. By use of the scaling theory of the localization, we will examine the behavior of the enhancement factor N_{eff} around the exciton mobility edge. The noticeable structure of the renormalized cooperon mode in Eq. (39) is that all the effect of disorder is incorporated only through the renormalized diffusion coefficient $D_0(1-\Delta)$. According to the insight from the nonlinear σ model treatment, this nature is based upon the nonvanishing of the average density of states at the mobility edge.[14–18] As the average state density of the exciton is not expected to vanish at the exciton mobility edge, we take full advantage of this feature as well as the scaling theory of the localization in order to evaluate the disorder effect on N_{eff}. When the inelastic-scattering length $L_\varphi = [N_0(-i\omega_s + i\omega_p + 2\gamma)]^{-1/d}$ is introduced, the enhancement factor N_{eff} and the coherent volume function Ξ_L are given by

$$N_{\text{eff}} = \frac{N}{V} \left[1 + \frac{1}{d} \frac{\partial}{\partial \ln L_\varphi} \right] \Xi_L, \tag{42}$$

$$\Xi_L = \frac{1}{N_0 D_L (q^2 + L^{-2}) + L_\varphi^{-d}}. \tag{43}$$

Here we omit the numerical factor $2/\pi$ as we are discussing only the order of magnitude. In Eq. (43) we carefully replaced q^2 by $q^2 + L^{-2}$, because all the momenta are discretized and cut off by the order of $1/L$ in the sample with finite volume $V = L^d$. The renormalized diffusion coefficient D_L also depends upon L, q, and L_φ, as will be discussed in the following. The length-dependent scaling theory[12] allows us to estimate the renormalized diffusion coefficient in terms of the dimensionless conductance $g_L = L^{d-2} N_0 D_L$. The dimensionless conductance g_L is determined by the following relation in the weakly localized regime,

$$L \frac{d \ln g_L}{dL} = \beta(g_L) = (d-2) - \frac{1}{g_L} + \cdots. \tag{44}$$

On the right-hand side, we made use of the result obtained by the expansion in $\epsilon = d - 2$. Thus we obtain

$$N_0 D_L = g_{L'} (L')^{2-d} = g^* \left[(L')^{2-d} + (\xi)^{2-d} \right], \tag{45}$$

on the delocalized side of the exciton mobility edge, where g^* is given by $1/(d-2)$. The correlation (localization) length ξ diverges at the mobility edge like

$|\omega - \omega^*|^{-\nu}$.[13,22] The critical exponent ν is between 0.73 (by ϵ expansion with the Borél-Padé analysis[23]) and $\sim$ 1.5 (by numerical analysis[24]). The length $L' \equiv \min[L, q^{-1}, L_\varphi]$ is the effective linear size of the system that $N_0 D_L$ is scaled up to. In the following, we shall consider only the three-dimensional case where the localized-delocalized transition is believed to occur. As a result, we obtain the expression for Ξ_L on the delocalized side of the transition as

$$\Xi_L = \left[\left(\frac{1}{\min[L, L_\varphi, q^{-1}]} + \frac{1}{\xi}\right)(q^2 + L^{-2}) + L_\varphi^{-3}\right]^{-1}. \tag{46}$$

We discuss all the effect due to disorder, misalignment, and finiteness of the sample, based upon Eq. (46). In the large volume limit, the behavior of N_{eff} for the phase-conjugated signal obtained from Eq. (46) is identical to that obtained in Ref. 8.

C. Sample size dependence

We investigate the sample size dependence of the coherent volume function Ξ_L in the case $\mathbf{q} = \mathbf{k}_f + \mathbf{k}_b = 0$ both on the sides of the exciton mobility edge. First we examine the behavior of Ξ_L on the delocalized side. As is easily confirmed from Eq. (46), the coherent volume function Ξ_L is proportional to L^3 in small linear size. The larger the linear size becomes, the more deviated the coherent volume function from the cubic power law and at last it is saturated to the constant value L_φ^3, as shown in Fig. 4. This crossover occurs at $L \sim L_\varphi$ and the behavior in the intermediate (mesoscopic) region is also highly dependent on the size of the correlation length ξ, as the solid lines in Fig. 4 show.

We now go on to the behavior on the localized side of the transition. When the localization length ξ is larger than the effective linear size $L' = \min[L, q^{-1}, L_\varphi]$ we cannot distinguish between the localized state and the delocalized state, so we expect that the behavior on the localized side is similar to that on the delocalized side.

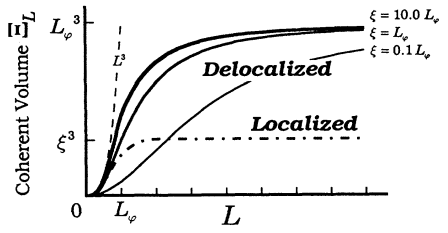

FIG. 4. The behavior of the coherent volume function Ξ_L as a function of the sample size L at $\mathbf{q} = \mathbf{k}_f + \mathbf{k}_b$. In the small volume limit, Ξ_L is proportional to L^3 (the dashed line) both in the delocalized side (the solid line) and the localized side (the dotted-dashed line) of the exciton mobility edge. The value of Ξ_L is saturated to L_φ^3 on the delocalized side, or to ξ^3 on the localized side. Approaching the exciton mobility edge from the delocalized side, Ξ_L increases as L^3 in the mesoscopic region but always saturated to L_φ^3 in the large volume limit both on the localized and delocalized sides.

However, when the localization length is smaller than $L' = \min[L, q^{-1}, L_\varphi]$, the difference between the localized and delocalized sides emerges. We can estimate Ξ_L on the localized side by following the scaling law away from the initial point near the fixed point up to a length scale $L = \xi$.[25] As a result, we expect that the coherent volume function Ξ_L on the localization sides is proportional to L^3 in the small volume limit and saturated to ξ^3, not to L_φ^3, as Fig. 4 shows.

D. Spectral anomaly and momentum dependence around the exciton mobility edge

Next we illustrate the expected behavior of N_{eff} in the unit of N/V as a function of ξ^{-1} and q in Fig. 5. Since the correlation (localization) length ξ is proportional to $|\omega - \omega^*|^{-\nu}$, Fig. 5(a) shows the anomalous ω dependence of the enhancement factor N_{eff} around the exciton mobility edge ω^* with the fixed misalignment q. Just near the transition point, the singularity is cut off

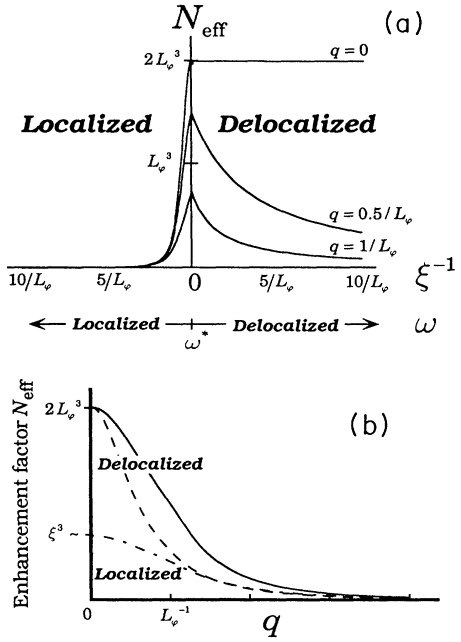

FIG. 5. The schematic behavior of the enhancement factor N_{eff} generating the phase-conjugated wave in the unit of N/V as a function of the inverse of the correlation (localization) length $\xi^{-1} \propto |\omega - \omega^*|^\nu$ or as a function of the misalignment of forward and backward pump beams $\mathbf{q} = \mathbf{k}_f + \mathbf{k}_b$ for a large sample size $L \gg q^{-1}, L_\varphi$. (a) N_{eff} as a function of ξ^{-1} for a large q and a small q. Since ξ is given by $\ell|(\omega - \omega^*)/\omega^*|^{-\nu}$, this figure corresponds to the spectrum anomaly around the mobility edge ω^*. On the localized side, N_{eff} decreases by $N_{\text{eff}} \sim \xi^3$, whereas N_{eff} does by $N_{\text{eff}} \sim \xi/q^2$ on the delocalized side, when the pumping frequency is far away from ω^*. (b) The behavior of N_{eff} as a function of q for a large sample. Near the exciton mobility edge (the solid line), the delocalized and the localized states cannot be distinguished. Away from the exciton mobility edge, the discrimination emerges between the delocalized side (the dashed line) and the localized side (the dotted-dashed line) for $q \lesssim L_\varphi^{-1}$.

by $\sim 2L_\varphi^3$ both on the sides. Away from the transition point, $N_{\rm eff}$ decreases as $\xi^3 \propto |\omega-\omega^*|^{-3\nu}$ on the localized side and as $\xi/q^2 \propto |\omega-\omega^*|^{-\nu}$ on the delocalized side, which makes the spectrum nonsymmetric on the tails. As shown by Fig. 5(a), it should be noted that when the misalignment q approaches zero, the region where $N_{\rm eff}$ is dominated by the length scale L_φ is much larger on the delocalized side. The background intensity comes from the terms neglected in our treatment.[8] The relative value of the peak to the background is of the order of $(L_\varphi/\xi_{\rm coh})^3 \sim \gamma'/\gamma$ ($\gg 1$) at the mobility edge.

In Fig. 5(b) the enhancement factor $N_{\rm eff}$ is drawn as a function of the misalignment q. In the region so close to the exciton mobility edge that the correlation (localization) length ξ becomes larger than the characteristic wavelength q^{-1} and the inelastic-scattering length L_φ, the localized and delocalized states cannot be distinguished as shown by the solid line in Fig. 5(b). Away from the exciton mobility edge, where $\xi \lesssim q^{-1}$, the difference in the q dependence of the enhancement factor $N_{\rm eff}$ on the delocalized side (the dash line) and on the localized side (the dotted dash line) will emerge, as is shown in Fig. 5(b).

VI. CONCLUSIONS

To summarize, we have constructed the scale description of the phase-conjugated wave generation under nearly resonant pumping of the Frenkel excitons in a disordered system and found the enhancement factor $N_{\rm eff}$ for a phase-conjugated wave on both sides of the exciton mobility edge. In a small volume region, our theory reproduces the result of the confinement effect. For the larger volume crystal, the qualitative difference between the delocalized state and the localized state has been manifested. The expected singular behavior of the spectrum around the exciton mobility edge has also been demonstrated as a function of the pumping frequency and the misalignment of the two pump beams. We propose two kinds of experiments to observe the singular behavior of $\chi^{(3)}$ near the exciton mobility edge ω^*. We confine ourselves to the case of degenerate four-wave mixing in a large crystal, i.e., ω_0 equals ω_p in the system with $L \gg L_\varphi,\ q^{-1}$. First, when we have the finite misalignment $\mathbf{q} = \mathbf{k}_f + \mathbf{k}_b$ fixed, the singular behavior of the generation of the phase-conjugated wavelike $N_{\rm eff} = (N/V)\xi q^{-2} \propto |\omega-\omega^*|^{-\nu}$ can be observed as a function of the pump frequency ω_0 on the delocalized side for $\xi \lesssim L_\varphi^3 q^2 \ll q^{-1}$. When the pump frequency ω_0 is detuned from the exciton mobility edge ω^* on the localized side, the signal will decay more rapidly as $N_{\rm eff} = (N/V)\xi^3 \propto |\omega-\omega^*|^{-3\nu}$. This dependence of the signal on the pump frequency is saturated in so close a pumping region as $\xi \gtrsim L_\varphi^3 q^2$ on the delocalized side, or as $\xi \gtrsim L_\varphi$ on the localized side. This crossover will be able to determine the absolute value of the correlation and localization length $\xi = \xi_0|(\omega-\omega^*)/\omega^*|^{-\nu}$. Second, when the detuning $|\omega-\omega^*|$ is fixed on the delocalized or localized sides, the correlation or localization length ξ will be determined by changing the misalignment q. In pumping localized excitons, the enhancement factor $N_{\rm eff}$ is saturated to the value $(N/V)\xi^3 \propto |\omega-\omega^*|^{-3\nu}$ for the smaller misalignment $q \lesssim \xi^{-1}$, whereas it decreases as q^{-3} for the larger misalignment $q \gtrsim \xi^{-1} \gtrsim L_\varphi^{-1}$. By observing this crossover, we will be able to determine the localization length ξ as a function of ω. On the other hand, when the misalignment q decreases on the delocalized side, the enhancement factor $N_{\rm eff}$ for the phase-conjugated signal increases as q^{-3} for $q \gg \xi^{-1} \gg L_\varphi^{-1}$ or as q^{-2} for $\xi^{-1} \gg q \gtrsim (\xi/L_\varphi^3)^{1/2}$ and is saturated to the value $N_{\rm eff} = (N/V)L_\varphi^3$ for the smaller misalignment $q \lesssim (\xi/L_\varphi^3)^{1/2}$. The crossover at $q \sim (\xi/L_\varphi^3)^{1/2}$ depends on the detuning $|\omega-\omega^*|$. Hence we expect the singular enhancement of the third-order optical processes, i.e., the generation of the phase-conjugated wave near the exciton mobility edge. In the reverse way of thinking, we will be able to study the localized-delocalized transition of an exciton by observing the singular spectrum of phase-conjugated wave generation as a function of pump and probe frequency around the exciton mobility edge ω^* and the misalignment of the forward and backward beams.

Note added in proof. The effective linear size that appeared in Eq. (46) is actually $\min[L, \tilde{L}_\varphi, q^{-1}]$, where $\tilde{L}_\varphi$ is defined by $\sqrt{D/(-i\delta\omega+2\gamma)}$ with the renormalized diffusion coefficient D. Around the mobility edge, $\tilde{L}_\varphi$ is given by $(g^*)^{1/d}L_\varphi$, so we used L_φ instead of $\tilde{L}_\varphi$. It is also noted that $\tilde{L}_\varphi$ is equal to $(g^*)^{1/2}L_\varphi\sqrt{L_\varphi/\xi}$ in the delocalized limit.

ACKNOWLEDGMENTS

The authors wish to thank T. Tokihiro and N. Nagaosa for many encouraging and helpful discussions. This research was supported by Grand-in-Aid for Scientific Research on Priority Area, "New Functionality Materials — Design, Preparation, and Control —," and "Electron Wave Interference Effect in Mesoscopic Structures" from the Ministry of Education, Science and Culture of Japan, and by NEDO's International Joint Research Program.

[1] E. Hanamura, Phys. Rev. B **37**, 1273 (1988).
[2] E. Hanamura, Phys. Rev. B **38**, 1228 (1988).
[3] J. Feldmann, G. Peter, E.O. Göbel, P. Dawson, K. Moore, and C. Foxon, Phys. Rev. Lett. **59**, 2337 (1987).
[4] E. Hanamura, Proc. SPIE **1268**, 96 (1990).
[5] E. Hanamura, Phys. Rev. B **39**, 1152 (1989).
[6] V.E. Kravtsov, V.I. Yudson, and V.M. Agranovich, Phys. Rev. B **41**, 2794 (1990).
[7] V.I. Yudson and P. Reineker, Phys. Rev. B **45**, 2073 (1992).
[8] N. Taniguchi and E. Hanamura, Solid State Commun. **85**, 843 (1993).
[9] N. Taniguchi and E. Hanamura, Phys. Lett. A (to be published).
[10] J. Hegarty, L. Goldner, and M.D. Sturge, Phys. Rev. B **30**, 7346 (1984).
[11] S.T. Cundiff, H. Wang, and D.G. Steel (unpublished).

[12]E. Abrahams, P.W. Anderson, D.C. Licciardello, and T.V. Ramakrishnan, Phys. Rev. Lett. **42**, 673 (1979).
[13]P.A. Lee and T.V. Ramakrishnan, Rev. Mod. Phys. **57**, 287 (1985).
[14]K.B. Efetov, A.I. Larkin, and D.E. Khmel'nitskii, Zh. Eksp. Teor. Fiz. **79**, 1120 (1980) [Sov. Phys. JETP **52**, 568 (1980)].
[15]S. Hikami, Phys. Rev. B **24**, 2671 (1981).
[16]A.J. McKane and M. Stone, Ann. Phys. (N.Y.) **131**, 36 (1981).
[17]K.B. Efetov, Adv. Phys. **32**, 53 (1983).
[18]E. Abrahams and P.A. Lee, Phys. Rev. B **33**, 683 (1986).
[19]R.F. Loring and S. Mukamel, J. Chem. Phys. **84**, 1228 (1986).
[20]Y.R. Shen, *The Principles of Nonlinear Optics* (Wiley, New York, 1984).
[21]E. Hanamura, Phys. Rev. B **46**, 4718 (1992).
[22]D. Vollhardt and P. Wölfle, Phys. Rev. Lett. **48**, 699 (1982).
[23]S. Hikami, Prog. Theor. Phys. Suppl. **107**, 213 (1992).
[24]B. Kramer, K. Broderix, A. MacKinnon, and M. Schreiber, Physica A **167**, 163 (1990).
[25]Y. Imry, Y. Gefen, and D. J. Bergman, Phys. Rev. B **26**, 3436 (1982)